ELSEVIER

Applied Catalysis A: General 198 (2000) 223–234

APPLIED CATALYSIS A: GENERAL

www.elsevier.com/locate/apcata

Naphthalene hydrogenation over $Pt/TiO_2–ZrO_2$ and the behavior of strong metal–support interaction (SMSI)

Chun-Mei Lu [a], Yu-Ming Lin [b], Ikai Wang [a,*]

[a] *Department of Chemical Engineering, National Tsinghua University, Hsinchu, Taiwan*
[b] *Energy & Resources Laboratories, Industrial Technology Research Institute, Hsinchu, Taiwan*

Received 5 August 1999; received in revised form 23 October 1999; accepted 12 November 1999

Abstract

Vapor-phase naphthalene hydrogenation over various supported Pt catalysts was studied in a continuous fixed-bed microreactor. Experimental results indicated that the catalytic activity of the catalyst strongly depended on the nature of the support and the pre-reduction temperature. Reaction order was independent of the support as the reaction was pseudo-first-order with respect to naphthalene in the temperature range studied. By comparing the apparent rate constant over various supported Pt catalysts, Pt supported on $TiO_2–ZrO_2$ (1 : 1) reduced at a low temperature showed the highest activity. For higher pre-reduction temperatures, $Pt/TiO_2–ZrO_2$ (1 : 1) exhibited the least suppression of H_2 uptake, due to a stabilization effect exerted by ZrO_2, which prevents the migration of TiO_x moieties and the blockage of the Pt surface. However, the apparent depression of the hydrogenation activity of high-temperature reduced $Pt/TiO_2–ZrO_2$ (1 : 1) was significantly greater than the suppression of its hydrogen uptake. Furthermore, the decreasing value of the hydrogenation activity relative to the hydrogen uptake demonstrates electron perturbations between the support and the Pt metal.

Keywords: $TiO_2–ZrO_2$; Naphthalene hydrogenation; SMSI

1. Introduction

Noble metal dispersed on an oxide support is used as the catalyst for hydrogenation reactions. The oxide supporting materials have included alumina, silica, and titania. The use of acidic supports has been found to enhance benzene hydrogenation rates over dispersed Pd [1,2]. Clearly, a better understanding of the effect of the support material on catalytic behavior is important and may provide guidance in choosing or designing a better catalyst for a specific reaction. Aromatic compound hydrogenation is sensitive to the support used, but neither the role of the support in this reaction nor the reaction mechanism on the metal surface has been unequivocally determined. Vannices' studies with Pd catalysts in benzene hydrogenation produced a reaction model explaining the enhanced activity over catalysts using more acidic supports [1,2]. This model proposed that benzene adsorbed on acid sites in the metal–oxide interfacial region could react with hydrogen spillover from the metal surface [1–7]. According to this mechanism, the hydrogenation activity of the supported metal catalyst was determined by three major factors. The first factor was the metal dispersion or exposed metal surface, which provided active sites for dissociated adsorption of hydrogen. The second factor

* Corresponding author. Tel.: +886-3-571-5131 x3651; fax: +886-3-572-4725.
E-mail address: ikwang@che.nthu.edu.tw (I. Wang)

0926-860X/00/$ – see front matter
PII: S0926-860X(99)00515-3

was the support, which provided active sites for adsorption of aromatic reactants. The third factor was the spillover rate of adsorbed atomic hydrogen, which determined the rate of surface reaction between those two adsorbed species.

The dispersion of metal was determined by the amount of hydrogen uptake. The uptake of hydrogen could be significantly affected by altering the pre-reduction temperature. At a high-reduction temperature, the dispersed metal particles agglomerated, thus suppressing the uptake of hydrogen. Sintering phenomena were extensively illustrated for the noble metal dispersed on non-reducible oxide supports such as Al_2O_3 or SiO_2 [8–11]. Although restoring the uptake of hydrogen through the irreversible sintering process is difficult, different behavior was observed when the reducible oxide, TiO_2, rather than Al_2O_3 was used as the support. The uptake of hydrogen on Pt/TiO_2 could be restored by reoxidation followed by low-temperature reduction. This phenomenon, including electronic and geometric effects [8–17], has been extensively investigated. Nevertheless, many researchers failed to distinguish the electronic effects from the geometric effects, labeling them together as 'strong metal–support interaction' (SMSI). This SMSI effect suppressed the hydrogen chemisorption capacity and reduced the catalytic activity of the metal in reactions such as the hydrogenation of hydrocarbons. The binary mixed oxide, TiO_2–ZrO_2, prepared by the coprecipitation method, showed different properties and catalytic activity from its component oxides, TiO_2 and ZrO_2 [18,19]. Maximum values for surface area, acidity and basicity appeared at equal components: a 1 : 1 ratio of oxides ($TiO_2 : ZrO_2 = 1 : 1$). The catalytic activity of dehydrogenation, dehydrocyclization and hydrogenolysis over this binary oxide had been previously investigated [18–20]. A strong correlation between the catalytic activities and the catalyst properties was reported according to various mole ratios of TiO_2/ZrO_2 [18,19].

This work investigates the electronic effect of Pt supported on the binary oxide TiO_2–ZrO_2 with various Ti/Zr ratios. Adding ZrO_2 to TiO_2 may prevent the migration of TiO_2 onto the metal surface, thereby maximally reducing the geometric effect. Hence, our results demonstrate the electronic effect without any disturbing geometric effect. Hydrogenation of naphthalene to tetralin and decalin is chosen as the model reaction because no side reaction such as hydrogenolysis or isomerization could occur at a mild reaction temperature. Furthermore, these reactions allow us to determine the effect of first ring hydrogenation and second ring hydrogenation on the rate constants simultaneously.

2. Experimental

2.1. Preparation of catalysts

TiO_2–ZrO_2 solids with different molar ratios of TiO_2 to ZrO_2 were prepared by coprecipitation from an anhydrous alcohol solution containing titanium tetrachloride (Showa, 99% purity) and zirconium tetrachloride (Showa, 99% purity) with aqueous ammonia (25%) [20]. The precipitate was allowed to stand at room temperature for 1 h. It was washed with deionized water, until no chloride ions were detected on addition of $AgNO_3$ solution to the filtrate, and then dried at 393 K for 12 h. The dried precipitate was heated from room temperature to 823 K at a rate of 3 K/min and calcined at 823 K in air for 2 h.

Pt/TiO_2–ZrO_2 catalyst, which contained 1 wt.% Pt, was prepared by the incipient wetness method. A pre-set amount of $Pt(NH_3)_4(NO_3)_2$ (Strem, 99% purity) aqueous solution was added to the calcined TiO_2–ZrO_2 solids to form an incipiently wetting 'waste' and allowed to stand at room temperature for 48 h. This 'waste' was dried at 393 K for 12 h and calcined in air at 823 K at 3 K/min. The other catalysts, Pt/Al_2O_3, Pt/TiO_2 and Pt/ZrO_2, were similarly prepared.

2.2. Hydrogen chemisorption measurement

Hydrogen chemisorption, i.e. H_2 uptake, over various catalysts was measured at room temperature in a greaseless high-vacuum glass system by a static adsorption method [46]. The high vacuum was achieved by operating a mechanical pump to 10^{-3} Torr (1 Torr = 133.3 Pa) and then a diffusion pump up to 10^{-5} Torr. The catalyst was first reduced in the same way as for the activity measurement. After reduction, the system was evacuated for 1 h at the final reduction temperature. The system was then

cooled at room temperature and the hydrogen adsorption isotherm was measured at 298 K. The hydrogen uptake at zero pressure, found by extrapolating the linear portion of the hydrogen isotherm, was assumed to represent the saturation coverage of the metal.

2.3. Reaction setup and experimental procedure

Hydrogenation of naphthalene over various catalysts was carried out in a continuous-flow fixed-bed micro-reactor. Naphthalene (Lancaster, 98% purity) was first dissolved in a solvent composed of cyclohexane (Tedia, HPLC grade) and 1,2,3,4-tetramethylbenzene (Aldrich, 95% purity). The weight ratio of naphthalene, 1,2,3,4-tetramethylbenzene and cyclohexane was 5/15/80. 1,2,3,4-Tetramethylbenzene was added to the synthetic feed to prevent the solidification of naphthalene on the outlet line of the reactor. When the conversion was lower than 80%, 1,2,3,4-tetramethylbenzene was not converted under the reaction conditions. Thus, 1,2,3,4-tetramethylbenzene played another role as internal standard for GC analysis. This synthetic feedstock was fed into the micro-reactor and vaporized before entering the catalyst bed. The catalyst was pretreated with air at 823 K for 2 h and reduced by hydrogen at elevated temperatures for 2 h. The reaction was carried out at between 503 and 543 K at a pressure of 3.1 MPa. The mole ratio of hydrogen over naphthalene was 40. Both feedstock and product streams were analyzed by a gas chromatograph equipped with a flame ionization detector (FID). The column chosen for analysis was Carbowax 20M. The mole fractions of naphthalene, tetralin and decalin in the product stream were obtained from the results of analysis. Since there were no side reactions, the conversion of naphthalene was calculated by $X = 1 - W_n/(W_n + W_t + W_d)$, where W_n is the mole fraction of naphthalene in the product stream, W_t that of tetralin and W_d that of decalin.

The fresh catalyst showed an activity drop at the beginning of the run. However, the conversion approach to a constant value after 12 h of time-on-stream and the reproducibility was very good for different loadings of fresh catalyst. Besides, the change of the catalyst activity was checked by repeating the first reaction condition at the end of the series of experiments with the same loading of the catalyst. No significant catalyst deactivation was observed.

3. Results and discussion

3.1. Influence of reduction temperature on H_2 uptake by supported Pt catalysts

The uptake of H_2 measured at room temperature is usually used to indicate the dispersion and/or exposed surface of the metal particles on the oxide support. The catalyst must be pre-treated in an atmosphere of hydrogen at elevated temperatures to initiate the hydrogenation activity of the supported metal catalyst. However, the H_2 uptake by the catalyst could be suppressed by increasing the pre-reduction temperature, due to the fact that the sintering of the metal or the migration of the partially reduced oxide onto the metal depended on the nature of the support.

Fig. 1 presents different H_2 uptake profiles as the reduction temperature is increased from 425 to 725 K. For non-reducible oxides, Al_2O_3 and ZrO_2, H_2 uptake profiles monotonically decreased with increasing reduction temperature. This type of decrease was attributed to the simple agglomeration of dispersed metal particles, i.e. the sintering effect. However, for the reducible oxides, TiO_2, TiO_2–ZrO_2 (3 : 1) and TiO_2–ZrO_2 (1 : 1), the profile of H_2 uptake versus reduction temperature showed a maximum according to the quantity of ZrO_2.

For the reducible oxide TiO_2, numerous investigations have confirmed the strong interaction between the Pt metal and the support (SMSI effect) [17,21,22]. In a reducing atmosphere, Ti^{4+} can be partially reduced to Ti^{3+} and TiO_2 oxides would become TiO_x. As shown in Fig. 1, the uptake of H_2 by Pt/TiO_2 was found initially to increase as temperature was raised from 425 to 475 K and then to decrease at higher temperatures. In a lower range of reduction temperatures, 425–475 K, the formation of TiO_x would interact with the electron field of Pt and a better dispersion of Pt metal was therefore observed. Further raising the reduction temperature causes the TiO_x fragments to migrate onto the surface of Pt, resulting in a decline in H_2 uptake. Thus, the measured H_2 uptake drastically decreased at a reduction temperature above 475 K. As seen in Fig. 1, the increase in ZrO_2 content shifts

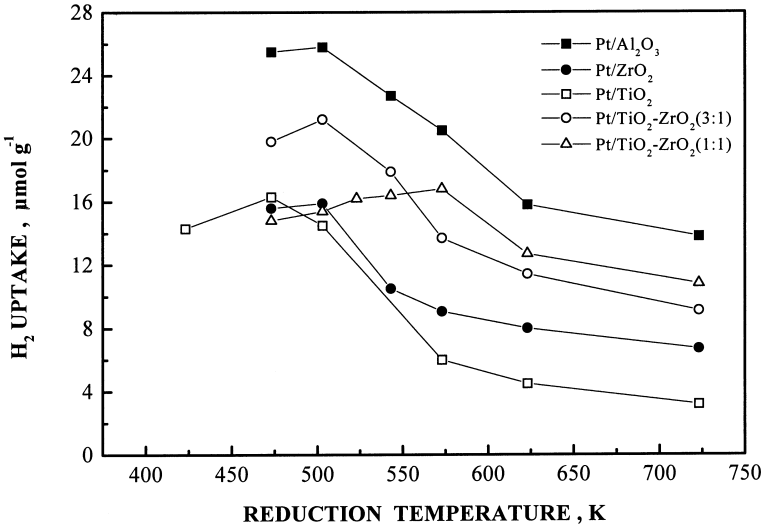

Fig. 1. Effect of reduction temperature on the hydrogen uptake over various catalysts.

the position of T_{max} (the temperature with the maximum hydrogen uptake) from 475 K (Pt/TiO_2) to 500 K (Pt/TiO_2–ZrO_2 (3 : 1)) and to 550 K (Pt/TiO_2–ZrO_2 (1 : 1)). These results imply a stabilization effect of ZrO_2 preventing the migration of TiO_x fragments that block the Pt surface for the uptake of hydrogen.

For convenience, three reduction temperatures were selected and denoted as LTR (low-temperature reduction, 503 K), MTR (medium temperature reduction, 623 K) and HTR (high-temperature reduction, 723 K). The amounts of H_2 uptake measured at 298 K for various supports at LTR, MTR and HTR are shown in Table 1. For comparison, a relative value of H_2 uptake referenced at LTR is also shown in parentheses. As shown in Table 1, all the values of relative H_2 uptake at MTR and HTR were smaller than unity. The decline in H_2 uptake by Pt/TiO_2 was clearly greater than for Pt/Al_2O_3 and Pt/ZrO_2, indicating the severe migration of TiO_x onto the Pt surface in high-temperature reduction. The relative amounts of H_2 uptake at MTR and HTR by the binary oxide, TiO_2–ZrO_2, were greater than the uptake by TiO_2 alone. For example, the relative H_2 uptake on Pt/TiO_2–ZrO_2 (1 : 1) at MTR and HTR were greater than 0.9, indicating the stabilization effect of ZrO_2.

The reversible property of the SMSI effect of TiO_2-containing catalysts is also illustrated in Table 1. After high-temperature reduction, the catalyst was reoxidized at 823 K and then retreated at LTR. The measured H_2 uptake is denoted as LTR(2) in Table 1.

Table 1
Amounts of H_2 adsorbed on the catalyst after low-, medium-, and high-temperature reductions[a]

Catalyst	Amount of H_2 adsorbed at 298 K (μmol/g catalyst)			
	LTR	MTR	HTR	LTR(2)
Pt/Al_2O_3	14.8 (1)	9.7 (0.66)	8.0 (0.54)	9.5
Pt/TiO_2	13.2 (1)	4.1 (0.31)	2.8 (0.21)	20.4
Pt/TiO_2–ZrO_2 (3 : 1)	16.2 (1)	7.0 (0.43)	6.1 (0.38)	21.3
Pt/TiO_2–ZrO_2 (1 : 1)	14.8 (1)	13.9 (0.94)	13.5 (0.91)	17.0
Pt/ZrO_2	10.9 (1)	5.4 (0.50)	4.7 (0.43)	5.8

[a] LTR: 503 K H_2 reduction; MTR: 623 K H_2 reduction; HTR: 723 K H_2 reduction; ( ): relative value. LTR(2): after HTR treatment, 823 K oxidation and then 503 K reduction.

The value of H_2 uptake was clearly restored (and even higher) for TiO_2-containing catalysts, demonstrating the reversible characteristics of the SMSI effect. In contrast, the H_2 uptake could not be restored for Al_2O_3 and ZrO_2, implying that such sintering is irreversible.

3.2. Activity of supported Pt catalysts for naphthalene hydrogenation

Naphthalene ($C_{10}H_8$) was hydrogenated to tetralin ($C_{10}H_{12}$) in the first step and then further hydrogenated to decalin ($C_{10}H_{18}$, *cis*- and/or *trans*-) according to the following scheme:

$$\underset{(C_{10}H_8)}{\text{Naphthalene}} \overset{2H_2,k_1}{\rightarrow} \underset{(C_{10}H_{12})}{\text{Tetralin}} \overset{3H_2,k_2}{\rightarrow} \underset{(C_{10}H_{18},cis\text{-}/trans\text{-})}{\text{Decalin}}$$

Hydrogenation was performed at a pressure of 3.1 MPa with a hydrogen/naphthalene mole ratio of 40. The reaction temperature was set between 503 and 543 K. Under such reaction conditions, there are no thermodynamic limitations for either naphthalene and tetralin [23–32]. Thus, the above scheme exhibits irreversible consecutive reaction behavior, i.e. $A \rightarrow B \rightarrow C$. Tetralin was produced as the intermediate product and decalin as the final product, that latter usually dominated by the *trans*-isomer. A typical product profile against 1/weight hourly space velocity (WHSV) is presented in Fig. 2. The reaction model was based on the following assumptions: (1) the reactor operated nearly isothermally; (2) intraparticle and interparticle transport resistances were negligible; (3) hydrogen was present in great excess and at a constant pressure, so the reversible reactions of hydrogenation were neglected. We assumed that the reaction mechanism of naphthalene hydrogenation followed the Langmuir–Hinshelwood model [6,33]. The rate-determining step was assumed to be the surface reaction between the adsorbed aromatic compounds and the dissociated hydrogen. The two reactants, hydrogen and the aromatic compounds, were adsorbed on separate active sites, i.e. dispersed metal and supporting oxide, respectively. According to these assumptions, the rate of hydrogenation can be expressed as

$$\text{Rate} = \frac{k' A_S K_N P_N}{(1 + K_N P_N + K_T P_T + K_D P_D + K_S P_S)} \times \frac{A_M K_H^{1/2} P_H^{1/2}}{(1 + K_H^{1/2} P_H^{1/2})} \quad (1)$$

where P_N, P_T, P_D, P_S and P_H are the partial pressures of naphthalene, tetralin, decalin, solvent and hydrogen, respectively; K_i is the adsorption constant for species i; A_M is the amount of metal active sites; A_S is the

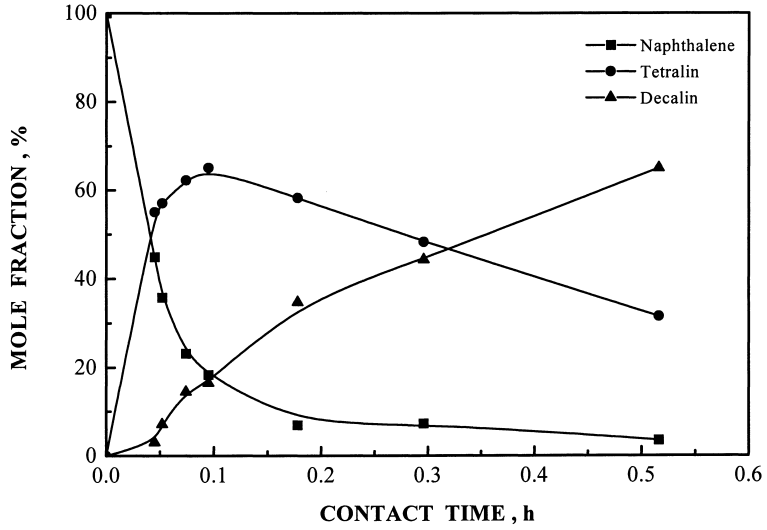

Fig. 2. Mole fraction vs. contact time profiles for naphthalene hydrogenation.

amount of oxide active sites; and k' is the rate constant of the reaction.

The partial pressure of hydrogen was almost constant during the reaction due to the large excess of hydrogen ($H_2/C_{10}H_8 = 40$ mole ratio). Therefore, the second part of Eq. (1) can be assumed to be constant. Furthermore, the concentration of naphthalene was only 5% in feed; the denominator in the first part of Eq. (1) could thus be regarded as a constant. Thus, the kinetic model of Eq. (1) can be rewritten in the form of a pseudo-first-order rate expression as

$$\text{Rate} = k_1 P_N \tag{2}$$

where k_1 is the apparent rate constant of naphthalene hydrogenation. Many researchers [34–36] also proposed this pseudo-first-order rate expression.

Inserting Eq. (2) into the material balance equation of a fixed bed reactor and integrating it, we obtain the design equation

$$-\ln(1 - X) = \frac{k_1}{\text{WHSV}} \tag{3}$$

where X denotes the conversion of naphthalene; k_1 is the apparent rate constant in h^{-1}; WHSV is the ratio of inlet flow rate over loaded catalyst in wt./wt./h. A plot of $\ln(1 - X)$ versus 1/WHSV yields a straight line with a slope of k_1, as illustrated in Fig. 3. The k_1 values of Pt/TiO_2 at 503, 523 and 543 K were calculated from the slope of each straight line. The k_1 values of different catalysts at different reaction temperatures were also calculated by the same method. As seen from Table 2, the hydrogenation activity of each catalyst decreased from LTR, through MTR, to HTR. To compare the extent of depression of k_1, we took the k_1 value at LTR as unity and calculated the relative values of k_1 at MTR and HTR. The results are shown in Table 2 and given in parentheses.

Arrhenius plots for the temperature dependence of the first-order rate constant

$$k = A \exp\left(\frac{-E_a}{RT}\right) \tag{4}$$

are presented in Fig. 4, where R is the gas constant. In Fig. 4, E_a was calculated from the slope. The apparent activation energies of naphthalene hydrogenation to tetralin were in the range of 11–22 kcal/mol. An activation energy larger than 6 kcal/mol may imply that the operation is in a reaction-controlled region [37]. The data further confirms that the reaction was reaction controlled. Significantly, the activation energy decreases slightly with the rise in pre-reduction temperature. Pt/TiO_2–ZrO_2 gives the lowest activation energy.

The primary product, tetralin, of naphthalene hydrogenation, is further hydrogenated to the final product, decalin, according to the above-mentioned

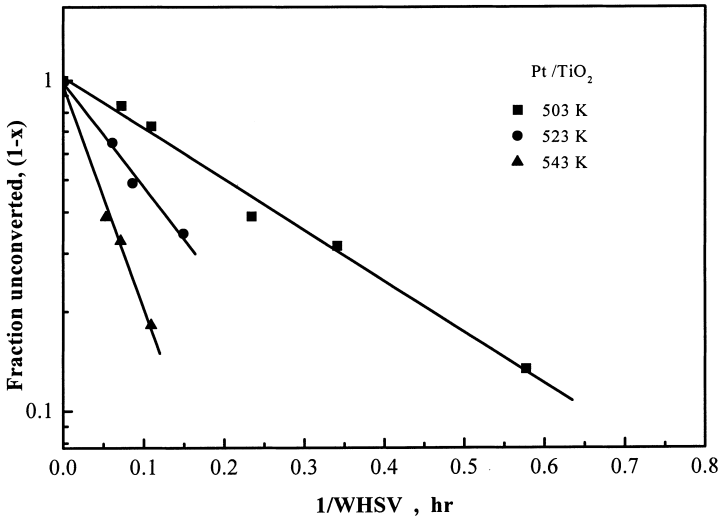

Fig. 3. Pseudo-first-order kinetics of naphthalene hydrogenation over Pt/TiO_2 at 3.1 MPa and H_2/naphthalene = 40.

Table 2
Rate constants and activation energies for the hydrogenation of naphthalene over the various catalysts after low-, medium-, and high-temperature reductions[a]

Catalyst	Treatment	k_1 at 503 K (h^{-1})	k_1 at 523 K (h^{-1})	k_1 at 543 K (h^{-1})	E_a (kcal/mol)
Pt/Al_2O_3	LTR	3.31 (1)	7.25 (1)	12.50 (1)	18.1
	MTR	2.35 (0.71)	4.84 (0.67)	8.12 (0.65)	16.9
	HTR	2.18 (0.66)	3.96 (0.55)	6.80 (0.54)	15.5
Pt/TiO_2	LTR	3.26 (1)	7.10 (1)	16.46 (1)	22.0
	MTR	2.23 (0.68)	4.43 (0.62)	10.00 (0.61)	20.4
	HTR	1.79 (0.55)	3.24 (0.46)	7.27 (0.44)	19.0
Pt/TiO_2–ZrO_2 (3 : 1)	LTR	6.38 (1)	14.90 (1)	26.26 (1)	19.3
	MTR	4.34 (0.68)	9.66 (0.65)	17.14 (0.65)	18.7
	HTR	2.65 (0.42)	5.24 (0.35)	9.93 (0.38)	18.0
Pt/TiO_2–ZrO_2 (1 : 1)	LTR	8.95 (1)	15.59 (1)	26.01 (1)	14.5
	MTR	6.15 (0.69)	10.55 (0.68)	15.82 (0.61)	12.9
	HTR	5.23 (0.58)	8.48 (0.54)	12.19 (0.47)	11.5
Pt/ZrO_2	LTR	1.18	2.62	5.66	21.3
	MTR	–	–	–	–
	HTR	–	–	–	–

[a] k_1: rate constant for $C_{10}H_8$ hydrogenation; E_a: Arrhenius activation energy; ( ): relative value.

reaction scheme. The pseudo-first-order kinetic model is also applicable to the hydrogenation of tetralin. The apparent rate constant, k_2, of this secondary hydrogenation, can be calculated from the following equation by a trial and error method:

$$P_D = P_{N0}\left[1 + \frac{1}{k_2 - k_1}(k_1 e^{-k_2 t} - k_2 e^{-k_1 t})\right] \quad (5)$$

Table 3 summarizes the calculated results of k_2 for each catalyst at LTR, MTR and HTR. As was the case for k_1, the k_2 value decreased as the pre-reduction temperature increased. Table 3 also contains the relative value of k_2. The values of E_{a_2} for various catalysts were obtained in the range of 13–16 kcal/mol. For a given catalyst, the activation energy is almost

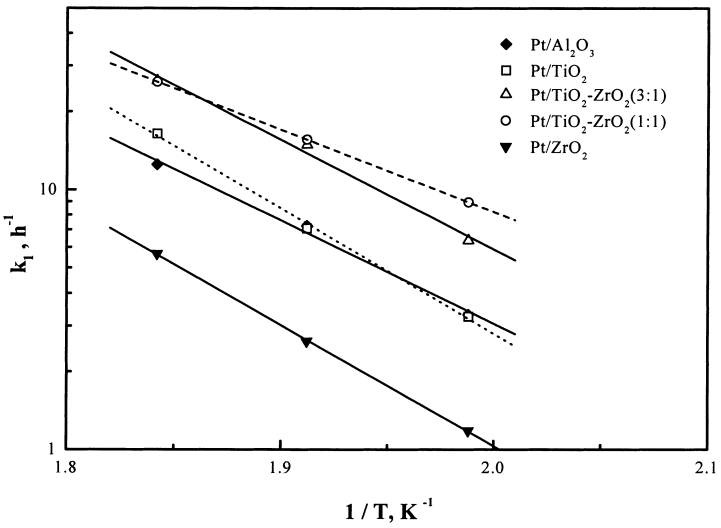

Fig. 4. Arrhenius plot for the rate constants k_1.

Table 3
Rate constants and activation energies for the hydrogenation of tetralin over the various catalysts after low-, medium-, and high-temperature reductions[a]

Catalyst	Treatment	k_2 at 503 K (h^{-1})	k_2 at 523 K (h^{-1})	k_2 at 543 K (h^{-1})	E_a (kcal/mol)
Pt/Al_2O_3	LTR	1.16 (1)	2.00 (1)	3.00 (1)	13.0
	MTR	0.75 (0.65)	1.29 (0.65)	1.90 (0.63)	12.7
	HTR	0.60 (0.52)	1.04 (0.52)	1.56 (0.52)	13.0
Pt/TiO_2	LTR	1.47 (1)	3.30 (1)	4.55 (1)	15.5
	MTR	0.88 (0.60)	2.02 (0.61)	2.80 (0.62)	15.8
	HTR	0.69 (0.47)	1.53 (0.46)	2.15 (0.47)	15.5
Pt/TiO_2–ZrO_2 (3 : 1)	LTR	2.40 (1)	4.08 (1)	6.50 (1)	13.6
	MTR	1.59 (0.66)	2.68 (0.66)	4.26 (0.66)	13.5
	HTR	0.95 (0.40)	1.62 (0.40)	2.59 (0.40)	13.7
Pt/TiO_2–ZrO_2 (1 : 1)	LTR	2.55 (1)	4.25 (1)	6.89 (1)	13.5
	MTR	1.90 (0.75)	3.00 (0.71)	5.08 (0.74)	13.4
	HTR	1.60 (0.63)	2.52 (0.59)	4.28 (0.62)	13.4
Pt/ZrO_2	LTR	0.30	0.60	0.85	14.1
	MTR	–	–	–	–
	HTR	–	–	–	–

[a] k_2: rate constant for $C_{10}H_{12}$ hydrogenation; ( ): relative value.

a constant, independent of the pre-reduction temperature. According to Tables 2 and 3, Pt/TiO_2–ZrO_2 gave the highest values of both k_1 and k_2. Notably, k_2 is always smaller than k_1, indicating that first ring hydrogenation is much faster than second ring hydrogenation. However, Pt/TiO_2–ZrO_2 supports the highest ratio of k_2 to k_1 as shown in Fig. 5. In practice, increasing the k_2 to k_1 value will improve the saturation of aromatics in deep hydrogenation diesel fuel.

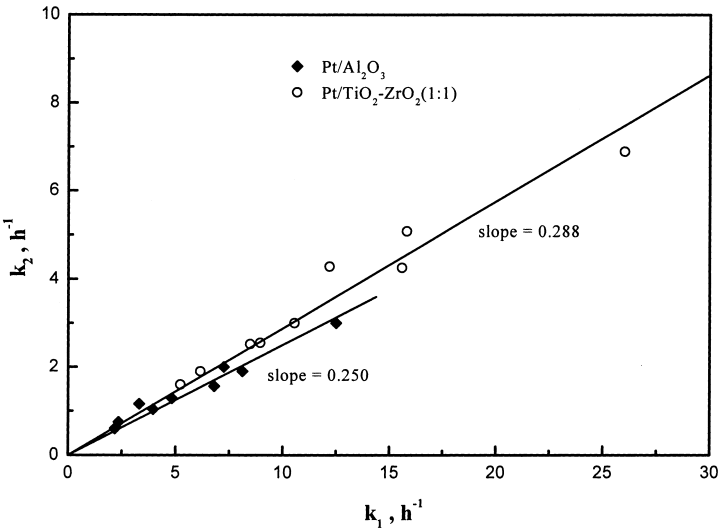

Fig. 5. The correlation of k_1 with k_2 for $Pt/A1_2O_3$ and Pt/TiO_2–ZrO_2 (1 : 1).

3.3. Correlation between hydrogenation activity and SMSI effect

The properties of the oxide used as support were believed to play an important role in the hydrogenation process. In a series of studies on benzene hydrogenation over the supported noble metal catalysts, Vannice et al. concluded that the use of acidic supports could enhance the rate of hydrogenation [1,2,4–6]. This positive effect was explained by an increased adsorption of benzene with increased acidity of support oxides. Similar results were found for the hydrogenation of naphthalene in the present work. According to Table 1, the H_2 uptakes of Pt over oxides containing TiO_2 were not significantly different from each other as the catalysts were pre-reduced at a temperature of 503 K. However, the rate constant k_1 clearly increased with increasing ZrO_2 content at a given reaction temperature, as shown in Table 2.

As reported by Wu et al. [18,19], the acidity of the mixed oxide, TiO_2–ZrO_2, reached a maximum value at a ZrO_2 content of 50%. This result clearly indicates that an increase in the acidity of the support enhances the hydrogenation activity, thereby allowing more aromatic reactant to be adsorbed.

As mentioned above, naphthalene is first adsorbed at metal–support interfacial sites, and is then reacted with spillover-hydrogen from Pt. The factors which determine rate constants are as follows: (i) the number of metallic active sites (A_M), (ii) the number of metal–oxide interfacial active sites (A_S), and (iii) the spillover rate of hydrogen. As seen in Fig. 6, the relative values of H_2 uptake versus the relative values of rate constant k_1 for Pt/Al_2O_3 almost meets the 'consistent line', indicating that the depression of activity was simply caused by the partial loss of the metal surface due to sintering in high-temperature reduction. The region above the consistent line indicates a loss of metal surface greater than the depression of activity and vice versa. The drop in relative k_1 for Pt/TiO_2 and Pt/TiO_2–ZrO_2 (3 : 1) was significantly smaller than that in their relative hydrogen uptakes. This fact follows from the migration of TiO_x onto the Pt surface, which in turn leads to a decrease in A_M but an increase in A_S. For Pt/TiO_2–ZrO_2 (1 : 1), the relative hydrogen uptake did not significantly fall after high-temperature reduction since ZrO_2 was very stable, preventing the migration of TiO_x fragments. In this situation, we might assume that there was no change in A_S or A_M. However, the drop of relative k_1 is obviously greater than the fall in relative hydrogen uptake, implying the electronic interaction between the support and the metal, which pulls the electrons from metal to oxide. It would retard the rate of spillover of hydrogen atoms. The diffusion of hydrogen atoms from the platinum particles to the surrounding support

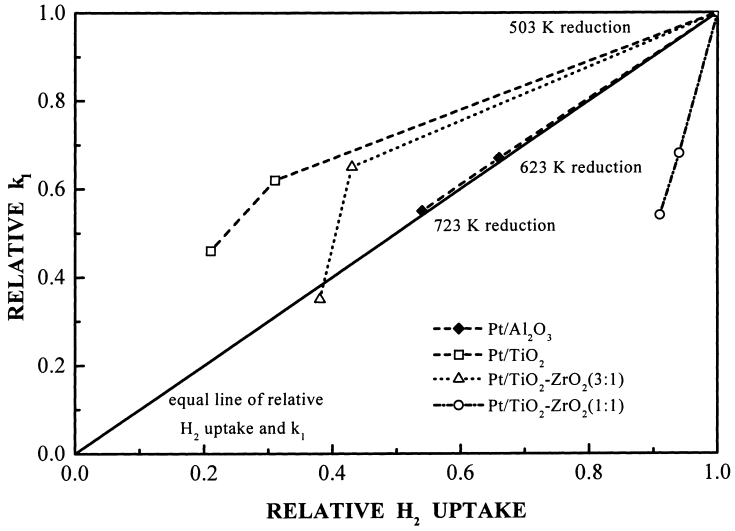

Fig. 6. The correlation of relative H_2 uptake with relative k_1 at 523 K of Pt supported on various oxides.

surface during the formation of protons and reduced titanium ions is related to the so-called spillover phenomenon. In Huizingas' studies, the results of an ESR study of platinum on TiO_2 are presented. Their results demonstrate that, at temperatures as low as 573 K, Ti^{3+} ions are formed presumably in the neighborhood of the platinum particles. The Ti^{3+} ions, when formed by a low-temperature reduction, can easily be retransformed into Ti^{4+} ions, but this is not the case for Ti^{3+} ions formed at 773 K [38].

The influence of hydrogen spillover on the hydrogenation of benzene has been reported in a number of articles [39–43]. Moreover, some researchers have concluded that the concentration of oxygen atoms (or hydroxyl groups) on the support surface affects the rate of hydrogen spillover [44–46]. The higher concentration of oxygen atoms implies a higher rate of hydrogen spillover.

The change of the surface structure of TiO_2–ZrO_2 during reduction treatment by H_2 has been proposed in the previous study of Wu et al. [18,19] as follows:

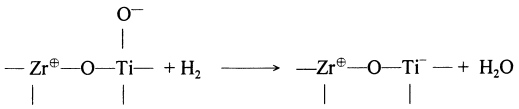

According to Wu, some oxygen atoms are removed by deep reduction. However, acidity and basicity of TiO_2–ZrO_2 (1 : 1) did not significantly change after reduction [18,19]. Therefore, the adsorptivity of the aromatic reactant should not decrease and thereby lead to a decline in reactivity. Correspondingly, the loss of reactivity of high-temperature reduced Pt/TiO_2–ZrO_2 (1 : 1) could be reasonably explained by the slowdown of hydrogen spillover, originating from the removal of oxygen atoms on the surface of the oxide support. The concentration of oxygen atoms decreases as the concentration of ZrO_2 increases because the structure of TiO_2–ZrO_2 is such that each oxygen atom is accompanied by a Ti atom. The hydrogen TPD profiles for the Pt/Al_2O_3 and Pt/TiO_2–ZrO_2 (1 : 1) catalysts after hydrogen reduction at different temperatures are given in Figs. 7 and 8. The desorption peak does not change when increasing the catalyst reduction temperature for Pt/Al_2O_3. In contrast, the desorption peak of Pt/TiO_2–ZrO_2 (1 : 1) is shifted to higher temperatures with increasing reduction temperature. This observation could explain the slowdown of hydrogen spillover. The decrease in activity should become more significant as the quantity of ZrO_2 is increased, as is demonstrated by the profiles in Fig. 6. The same conclusion follows from the correlation of relative H_2 uptake versus the rate constant k_2 for the secondary hydrogenation of tetralin, when the data in Table 3 are rearranged in a manner similar to those in Fig. 6.

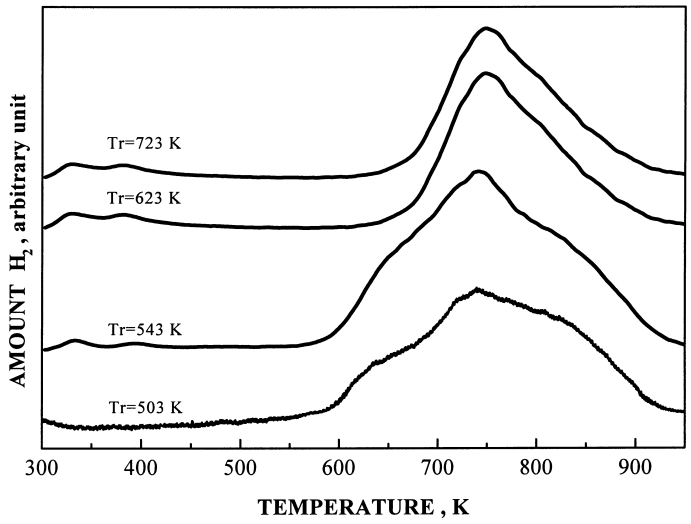

Fig. 7. The H_2-TPD of Pt/Al_2O_3, at different reduction temperatures.

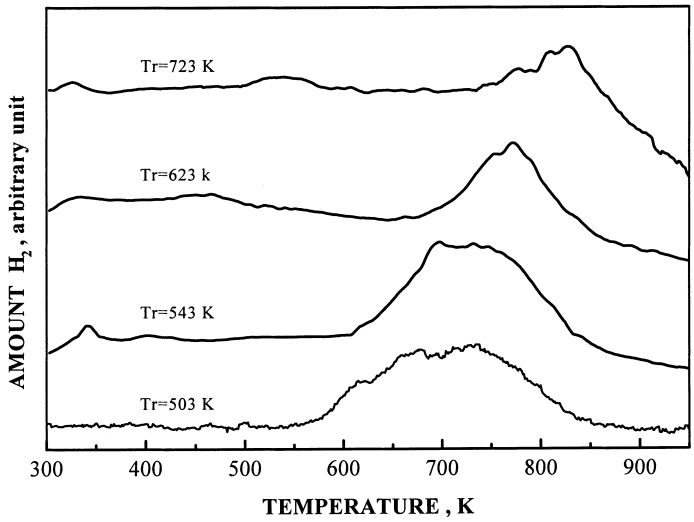

Fig. 8. The H_2-TPD of Pt/TiO_2–ZrO_2 (1 : 1), at different reduction temperatures.

4. Conclusion

Based on above discussion, we can conclude the following:

1. Pt/TiO_2–ZrO_2 significantly influences the interaction between the metal and the support. The existence of ZrO_2 plays an important role in preventing both the migration of reduced TiO_x moieties and the blockage of the metal surface (the geometric effect), so that a supported Pt catalyst such as Pt/TiO_2–ZrO_2 (1 : 1) retains the H_2 uptake even throughout the high-temperature reduction.
2. A pseudo-first-order kinetic model was established to illustrate the reactivity of each supported Pt catalyst for naphthalene hydrogenation. Pt/TiO_2–ZrO_2 (1 : 1) showed the highest activity among all supported Pt catalysts.
3. Correlating the relative H_2 uptake with the relative rate constant for the Pt/Al_2O_3 catalyst was consistent due to the sintering of dispersed Pt particles. The Pt/TiO_2–ZrO_2 (1 : 1) catalyst showed a great depression in hydrogenation activity by high-temperature pre-reduction, despite exhibiting the highest relative H_2 uptake. This depression of activity might be explained by the slowdown of hydrogen spillover.

Acknowledgements

The authors would like to thank the Refining and Manufacturing Research Center of the Chinese Petroleum Corporation for financially supporting this research.

References

[1] P. Chou, M.A. Vannice, J. Catal. 107 (1987) 129.
[2] P. Chou, M.A. Vannice, J. Catal. 107 (1987) 140.
[3] J.M. Basset, I.G. Dalmai, M. Primet, R. Matin, J. Catal. 37 (1975) 22.
[4] M. Boudart, A.W. Aldog, M.A. Vannice, J. Catal. 18 (1970) 46.
[5] S.D. Lin, M.A. Vannice, J. Catal. 143 (1993) 539.
[6] S.D. Lin, M.A. Vannice, J. Catal. 143 (1993) 563.
[7] T.C. Huang, B.C. Kang, Ind. Eng. Chem. Res. 34 (1995) 1140.
[8] J. Santos, J. Phillips, J.A. Dumesic, J. Catal. 81 (1983) 147.
[9] H.R. Sadeghi, V.E. Henrich, J. Catal. 87 (1984) 279.
[10] Y.M. Sun, D.N. Belton, J.M. White, J. Phys. Chem. 90 (1986) 5178.
[11] T. Yokoyama, K. Asakura, Y. Iwasawa, H. Kuroda, J. Phys. Chem. 93 (1989) 8323.
[12] S.T. Tauster, S.C. Fung, R.L. Garten, J. Am. Chem. Soc. 100 (1978) 170.
[13] S.T. Tauster, S.C. Fung, R.T.K. Baker, J.A. Horsley, Science 211 (1981) 1121.

[14] T.M. Salama, H. Hattori, H. Kita, K. Ebitani, T. Tanaka, J. Chem. Soc., Faraday Trans. 89 (1993) 2067.
[15] P.R. Madhusudhan, B. Viswanathan, R.P. Viswanath, J. Mater. Sci. 30 (1995) 4980.
[16] G.R. Rao, C.N.R. Rao, J. Phys. Chem. 94 (1990) 7986.
[17] A.D. Logan, E.J. Braunschweig, A.K. Datye, D.J. Smith, Langmuir 4 (1986) 827.
[18] I. Wang, W.F. Chang, R.J. Shiau, J.C. Wu, C.S. Chung, J. Catal. 83 (1983) 428.
[19] J.C. Wu, C.S. Chung, C.L. Ay, I. Wang, J. Catal. 87 (1984) 98.
[20] J. Fung, I. Wang, J. Catal. 130 (1991) 577.
[21] L. Bonneviot, G.L. Haller, J. Catal. 130 (1991) 359.
[22] A.C. Faro Jr., C. Kemball, J. Chem. Soc., Faraday Trans. 91 (1995) 741.
[23] R.C. Reid, J.M. Prausnitz, T.K. Sherwood, The Properties of Gases and Liquids, McGraw-Hill, New York, 1977.
[24] S.B. Jaffe, Kinetics of heat release in petroleum hydrogenation, Ind. Eng. Chem. Process Des. Dev. 13 (1974) 34.
[25] C.G. Frye, J. Chem. Eng. Data 7 (1962) 592.
[26] C.G. Frye, A.W. Weitkamp, J. Chem. Eng. Data 14 (1969) 372.
[27] D.R. Stull, E.F. Westrum, G.C. Sinke, The Chemical Thermodynamics of Organic Compounds, Wiley, New York, 1969.
[28] T.P. Wilson, E.G. Caflisch, G.F. Hurley, J. Phys. Chem. 62 (1958) 1059.
[29] R. Shaw, D.M. Golden, S.W. Benson, J. Phys. Chem. 81 (1977) 1716.
[30] S. Stein, D.M. Golden, S.W. Benson, J. Phys. Chem. 81 (1977) 314.
[31] L.F. Lepage, Applied Heterogeneous Catalysis, Technip, Paris, 1987.
[32] A.J. Gully, W.P. Balard, in: J.J. McKetta, Jr. (Ed.), Advances in Petroleum Chemistry and Refining, Vol. 7, Interscience, London, 1963, p. 241.
[33] P.C. Aben, J.C. Platteeuw, B. Stouthamer, in: Proc. 4th Int. Congr. on Catalysis, (paper 31), Vol. 1, 1968, p. 395.
[34] A.V. Sapre, B.C. Gates, Ind. Eng. Chem. Process Des. Dev. 20 (1981) 68.
[35] C. Chu, I. Wang, Ind. Eng. Chem. Process Des. Dev. 21 (1982) 338.
[36] M. Koussathana, N. Vamvouka, X.E. Verykios, Appl. Catal. A: Gen. 95 (1993) 211.
[37] G.C. Bond, Heterogeneous Catalysis: Principles and Applications, 2nd Edition, Oxford University Press, Oxford, 1987, pp. 57–60.
[38] T. Huizinga, R. Prins, J. Phys. Chem. 85 (1981) 2156.
[39] J.L. Carter, in: Proc. 3rd Int. Congr. on Catalysis, Amsterdam, 1964, Wiley, New York, 1965, p. 1.
[40] K.M. Sancier, J. Catal. 20 (1971) 106.
[41] P. Antonucci, N.V. Truong, N. Giordano, R. Maggiore, J. Catal. 75 (1982) 140.
[42] S. Ceckiewicz, B. Delmon, J. Catal. 108 (1987) 294.
[43] S.T. Srinivas, P.K. Rao, J. Catal. 148 (1994) 470.
[44] G.L. Haller, E. Resasco, Adv. Catal. 36 (1989) 173.
[45] S. Bernal, J.J. Calvino, G.A. Cifredo, A. Laachir, V. Perricho, J.M. Hermann, Langmuir 10 (1994) 717.
[46] S.C. Chou, C.T. Yeh, T.H. Chang, J. Phys. Chem. B 101 (1997) 5828.